







RESEARCH ARTICLE | DECEMBER 29 2023

## Pinching dynamics and extensional rheology of dense colloidal suspensions with depletion attractions

Diego D. Soetrisno ; Carina D. V. Martínez Narváez ; Mariah J. Gallegos ; Vivek Sharma ; Jacinta C. Conrad  

 Check for updates

*J. Rheol.* 68, 99–112 (2024)

<https://doi.org/10.1122/8.0000717>



View  
Online



Export  
Citation

CrossMark



Advance your science, career  
and community as a member of  
**The Society of Rheology**

LEARN MORE





# Pinching dynamics and extensional rheology of dense colloidal suspensions with depletion attractions

Diego D. Soetrisno,<sup>1</sup> Carina D. V. Martínez Narváez,<sup>2</sup> Mariah J. Gallegos,<sup>1</sup> Vivek Sharma,<sup>2,a)</sup> and Jacinta C. Conrad<sup>1,b)</sup>

<sup>1</sup>*Department of Chemical and Biomolecular Engineering, University of Houston, Houston, Texas 77204*

<sup>2</sup>*Department of Chemical Engineering, University of Illinois Chicago, Chicago, Illinois 60607*

(Received 1 July 2023; final revision received 19 November 2023; published 29 December 2023)

## Abstract

We study the extensional flow properties by characterizing the capillarity-driven pinching dynamics of dense colloidal suspensions at a constant volume fraction  $\phi = 0.40$  with polymer-induced depletion interactions using a dripping-onto-substrate (DoS) protocol. Methacrylate copolymer particles with dimethylacrylamide copolymer brushes are suspended in a refractive-index- and density-matched mixture of 80 (w/w)% glycerol in water with NaCl added to screen the electrostatic repulsions. Depletion attractions between the colloids are introduced by adding polyacrylamide polymers of weight and dispersity. The addition of polymer delays and modifies the pinch-off dynamics of the dense suspensions, depending on the size and dispersity of the polymer. The extensional relaxation time  $\lambda_E$  of suspensions collapses as a function of the normalized free volume polymer concentration  $c/c^*$  with the corresponding polymer solutions, indicating that the elastic properties of the polymer solutions control the extensional time scale. Following the results of our previous study [Soetrisno *et al.*, *Macromolecules* **56**, 4919–4928 (2023)], the polymer size determines the scaling exponent of  $\lambda_E$  for colloid-polymer mixtures in the dilute regime and high dispersity shifts the concentration where the scaling of  $\lambda_E$  transitions from power-law to linear. The filament lifespans  $t_f$  of colloid-polymer mixtures and of polymer solutions collapse onto a master curve as a function of  $c/c^*$  when normalized by the filament lifespan of the corresponding fluid without polymer  $t_{f,0}$ . These results provide insight into the role of the polymer size in dictating the pinching dynamics and extensional rheology of colloid-polymer mixtures and further suggest that the shear and extensional responses of these mixtures can be separately tuned through the concentrations of the two constituents. © 2023 Published under an exclusive license by Society of Rheology. <https://doi.org/10.1122/8.0000717>

## I. INTRODUCTION

Designing particle-laden complex fluids for advanced material processing applications, including 3D printing [1–5], inkjet printing [6], coating [7,8], and electrospinning [9,10], requires understanding of their rheological responses in shear and extensional flows. The key rheological properties for these materials, including yield stress, elastic modulus, rate-dependent shear or extensional viscosity, and stringiness [11], are controlled through complex fluid composition [8,12,13]. One common class of feedstocks is a mixture of colloidal particles at high concentration and polymers. Feedstocks for printing, for example, include ceramic [14,15], metallic [16,17], food [18], and biomaterial [19] suspensions. Nonadsorbing polymers are commonly used as binders in printing and coating formulations [20–22]. Furthermore, they can mitigate shear-induced migration in confined flow geometries [23] involving mixed flows where the extensional material response is important. Polymers undergo significant stretching in response to extensional flows, exhibiting a strain-hardening extensional viscosity that can be significantly larger than the shear viscosity. Likewise,

polymer additives profoundly influence printing, coating, and fiber spinning operations, where strong extensional deformation arises within stretched liquid bridges and necks undergoing pinching during drop formation and dispensing [24–26]. These examples highlight the practical need to understand and control the extensional flow of mixtures of colloids and nonadsorbing polymers.

Most studies of the extensional rheology of particle-laden fluids focus on noncolloidal suspensions without added polymer (Table I) [27–43,50]. Two characteristic regimes were exhibited in response to capillarity-driven pinching and elongational flows in these studies: an initial response by the bulk viscosity; later, they accelerate to the interstitial fluid viscosity or even exceed the medium speed [31,37]. Strongly shear-thickening suspensions exhibit strain-dependent responses including Newtonian, elastic, and ductile fracture under filament stretching, whereas capillary breakup leads to an abrupt slowing of the radius evolution [51].

Despite the prevalence of extensional flows during use and processing of complex fluids [5,7,24,25], factors controlling the extensional response of particle-laden viscoelastic fluids (containing polymers) remain actively debated [13,52,53]. Simulations of noncolloidal suspensions in viscoelastic media show that the extensional rheology of the suspending fluid influences both shear and extensional rheology responses of the mixtures due to particle-induced stresses [54–56]. Experiments on noncolloidal particles (radii ranging from

<sup>a)</sup>Electronic mail: viveks@uic.edu

<sup>b)</sup>Author to whom correspondence should be addressed; electronic mail: jconrad@uh.edu

**TABLE I.** Literature review on capillary-driven pinching dynamics (drop detachment or capillary breakup experiments) of fluids containing spherical particles.

Particle	$a$ ( $\mu\text{m}$ )	$\phi$	$\eta_m$ (Pa·s)	$\gamma_m$ (mN/m)	$\rho_m$ ( $\text{kg/m}^3$ )	Medium	Ref.
PS, Iron, Acrylic, Glass	97–500	0.57–0.61	0.001–1	72, $\sim 21$	$\sim 1000$	Water, silicone oil	[27]
ZrO <sub>2</sub> , PS, PE, Glass	11–425	0.59–0.63	0.001, 0.02	72, $\sim 21$	$\sim 1000$	Water, silicone oil	[28]
PMMA	106–125	0.02–0.40	0.4	49	1184	Water, ZnCl <sub>2</sub> , PAG	[29]
PS	20–140	0.01–0.55	0.18	21	1070	Silicone oil	[30–33]
PS	10–250	0.02–0.50	0.12, 2.5	24, 45	1050–1060	Silicone oil, PEG	[34,35]
Glass	17–180	0.18–0.48	0.336	62.4	1240	95% Glycerol in water	36
PS	10–20	0.02–0.40	0.18–0.36	21	970–1070	Silicone oils	[37,38]
PMMA	5	0.04–0.17	0.01–0.10	21	1070	Silicone oils	[39,40]
PMMA	3	0.02–0.40	0.18–0.36	21.0	970–1070	Silicone oils	[37]
PMMA	0.60–1	0.59–0.63	0.004	30	789	Octadecene	[41,42]
PMMA	0.14–0.69	0.56–0.60	0.015	29.2	848	Squalene	[43]
PS	10–70	0.10–0.40	0.2	60	1057	300 kDa PEO in G/W	[44,45]
PS	20	0.05–0.20	2.2	72	1352	5 MDa PAA in corn syrup mix	[46,47]
PMMA	3	0.15–0.40	0.1–0.9	70	997	35 kDa PEG in water	[48]
PMMA	0.5	0.02–0.09	0.02	60	997	2 MDa PEO in water	49

$3\ \mu\text{m} < a < 70\ \mu\text{m}$ ), however, reveal contrasting effects of particle addition. For polystyrene particles in poly(ethylene oxide) solutions, the viscoelastic medium dominates the extensional response of the mixtures [44], similar to the interstitial fluid picture in Newtonian fluids. By contrast, depletion attractions between poly(methyl methacrylate) particles in poly(ethylene glycol) solutions increase the viscoelastic response of the mixtures above that of the corresponding polymer solutions without added polymers [48]. Polystyrene particles added to a Boger fluid enhance strain hardening in filament-stretching experiments, and the magnitude is similar to the enhancement of shear viscosity [57]. Finally, increasing the concentration of polystyrene particles reduces the strain rate of poly(acrylic acid) in corn syrup/glycerol/water mixtures in a drop detachment experiment [46]. The disparity between these experimental observations may occur because the studies examine different regimes of polymer size and concentration, which has not been systematically investigated.

As the particle size enters the colloidal regime, Brownian motion affects the suspension rheology. Strongly shear-thickening colloidal suspensions have similar extensional properties to those of larger non-Brownian particles [41,58]. When the time scale of the filament breakup exceeds the Brownian time scale, however, the extensional properties of suspensions of Brownian particles differ [43], suggesting that Brownian motion contributes to the extensional response in a colloidal suspension.

Experimental studies of the extensional flow of colloidal (Brownian) particles in viscoelastic media focus on melts [59], on solutions in which the polymer adsorbs on the particle surfaces [60], or on practically relevant formulations where the interparticle interactions are not precisely known [7,61]. Intriguingly, in suspensions of Brownian PMMA particles in semidilute solutions of PEO, addition of particles at low concentrations (up to 10 wt.%) slightly increases the extensional viscosity and the extensional relaxation time set

by the polymers [49]. These results suggest that understanding of the extensional behavior of polymer solutions is essential for controlling the extensional properties of colloid-polymer mixtures.

Toward this end, a recent study of the extensional response of polymer solutions reveals that conformational changes under extensional flow control the scaling behavior of the extensional relaxation time with polymer concentration,  $\lambda_E \sim c^k$ , in the dilute regime [62]. The magnitude of  $k$  depends on the influence and extent of screening of the excluded volume interactions and is correlated with coil-stretch hysteresis, as demonstrated for polymers of different flexibility [62] or molecular weight distributions [63].

The influence of polymer size and concentration and molecular weight- or flexibility-dependent conformational changes on the extensional rheology of colloidal particle-polymer mixtures, however, has not yet been examined. In a previous study of shear rheology of colloidal particle-polymer mixtures at volume fraction  $\phi = 0.40$ , we found that shear thickening depends on polymer size [64]. Thereafter, we examined how polymer size affects the concentration-dependent extensional response in the dilute and semidilute particle-free polymer solutions [63]. Now, we hypothesize that polymer size will also influence the extensional response of colloid-polymer mixtures in a similar regime of polymer concentration.

To test this hypothesis, we characterize the extensional flow properties of dense suspensions of Brownian particles at a volume fraction of  $\phi = 0.40$  containing polyacrylamide (PAM) polymers, which induce short-ranged depletion interactions [64,65], of various molecular weight distributions. In polymer solutions, the responses to the extensional flow are dictated by their macromolecular properties [62], which can be derived from their monomer chemical structures and shear rheology characterization. Here, we vary the molecular weight of PAM to tune the macromolecular contributions to

the pinch-off dynamics of depletion suspensions. The concentration-dependent extensional properties of the depletion suspensions are dominated by contributions from the polymer additives when scaled with free volume concentration, suggesting that the polymer solution acts as an interstitial fluid under extensional flow. The filament lifespans for both polymer solutions and depletion suspensions increase with the addition of polymer and collapse onto a master curve when normalized by the lifespan of a corresponding zero-polymer fluid, indicating that polymer contributions are similar in polymer solutions and depletion suspensions. The results from this study provide insight into the role of polymer size on the extensional response for suspensions formulated at the high particle volume fractions used in printing applications [15,16]. Because the polymer contribution dominates the pinching dynamics and extensional response, our results also suggest that the shear and extensional responses of colloid-polymer mixtures can be separately tuned through the concentrations of particles and polymers.

## II. MATERIALS AND METHODS

### A. Materials

We synthesized poly(2,2,2-trifluoroethyl methacrylate-co-*tert*-butyl methacrylate) (TtMA) particles [66] that were refractive-index- and density-matched to 80 (w/w)% glycerol/water [65]. The colloidal particles (particle radius  $a = 900 \pm 40$  nm, dispersity  $\mathfrak{D} = 0.07$ ) had a fluorescent core and nonfluorescent shell architecture and bore a charged copolymer brush to provide electrostatic stabilization [Fig. 1(a)]. We estimated the average interparticle spacing between particles from  $h = 2a \left[ \left( \frac{\pi}{3\sqrt{2}\phi} \right)^{1/3} - 1 \right]$  [67].

The particle size was characterized using dynamic light scattering (DLS). Intensity-intensity correlation functions were acquired on an ALV-GmbH instrument (Langen, Germany) and a 5000 EPP Multiple tau Digital Correlator. The particle size was determined by fitting the intensity-intensity correlation function with a single exponential decay,

$$g^{(2)}(\tau, q) - 1 = \beta \exp(-2\Gamma\tau) \left( 1 + \frac{\mu_2}{2} \tau^2 \right), \quad (1)$$

where  $\beta \approx 1$  is a geometric correction factor,  $\Gamma$  is the decay rate,  $\tau$  is the lag time,  $q$  is the wavevector, and  $\mu_2$  is the second cumulant. We calculated the diffusion coefficient  $D = \Gamma q^{-2}$  and obtained the hydrodynamic diameter from  $2a = k_B T / 3D\pi\eta_s$ . We determined the dispersity via  $\mathfrak{D} = \mu_2 / \Gamma^2$ .

To generate short-ranged depletion attractions between the particles, we added polyacrylamide (PAM) polymers [Figs. 1(b) and 1(c)]. Three different PAMs with various molecular weight and dispersity were used:  $M_w = 194$  kDa,  $\mathfrak{D} = 1.24$ ,  $c^* = 12$  mg·mL<sup>-1</sup>,  $R_g = 19$  nm, Polymer Source, (denoted as USP, uniform small polymer);  $M_w = 1.00$  MDa,  $\mathfrak{D} = 1.25$ ,  $c^* = 3.2$  mg·mL<sup>-1</sup>,  $R_g = 50$  nm, Polymer Source (ULP, uniform large polymer); and  $M_w = 1.97$  MDa,  $\mathfrak{D} = 21$ ,  $c^* = 5.1$  mg·mL<sup>-1</sup>,  $R_g = 75$  nm, Sigma-Aldrich (DP, disperse polymer), all previously studied in [63]. The polymer properties are summarized in Table II.

The overlap concentration  $c^* = 1/[\eta]$  was calculated using the intrinsic viscosity  $[\eta]$  determined from the polymer solution shear rheology. The polymer  $R_g$ , estimated from  $c^*$ , satisfied  $R_g/a < 0.1$  for all three polymers, yielding short-range attractions [68]. The polymer concentration in suspensions was calculated as the concentration in the free volume (i.e., the volume accessible to the centers of the polymers) [69–71].

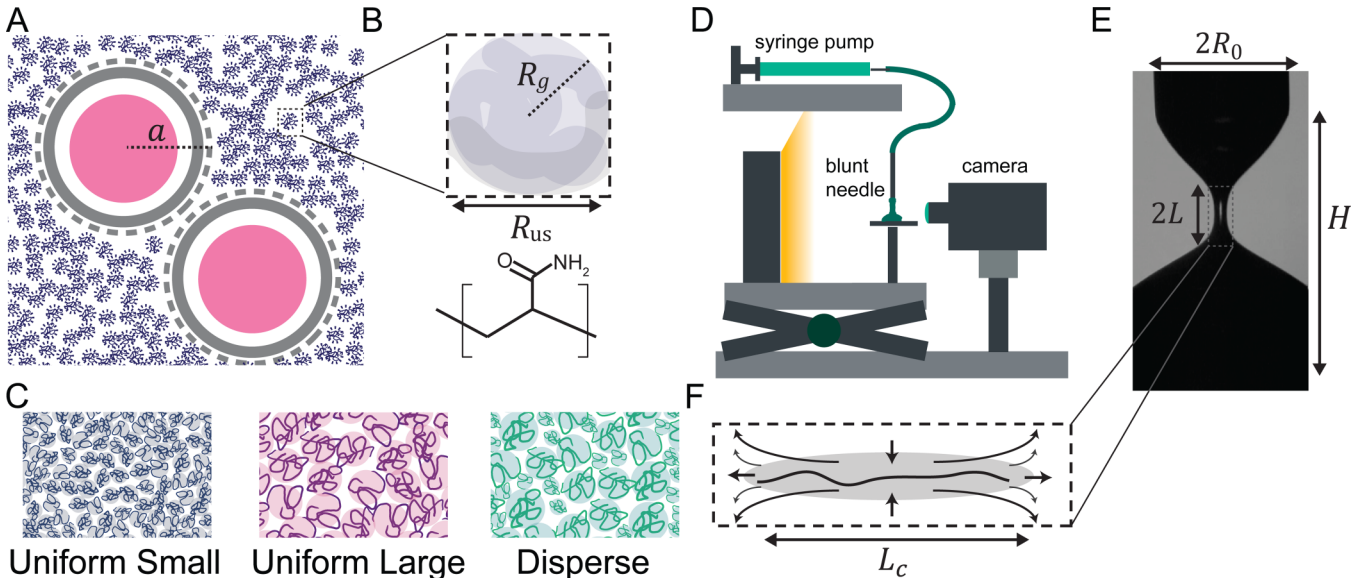


**FIG. 1.** (a) Illustration of depletion suspensions, which contain core-shell particles stabilized by polyelectrolyte brushes (radius  $a$ ) and polyacrylamide (PAM) polymers (radius  $R_g$ , with  $R_g \ll a$ ) that are suspended in an index- and density-matching glycerol/water solvent. (b) Enlarged illustration of the chemical structure of a PAM molecule and quiescent length scale (coiled length  $R_{us}$ ) (not shown to scale). (c) Schematic diagrams of three polymers with various molecular weight and dispersity used in this study: uniform small polymer (USP), uniform large polymer (ULP), and disperse polymer (DP). (d) Schematic of the DoS setup used in this study, which includes high-speed imaging over time of a polymer solution liquid bridge undergoing a capillary-driven instability. (e) An enlarged snapshot of the liquid bridge during measurement and the corresponding geometric length scales (nozzle radius  $R_0$ , distance from nozzle to substrate  $H$ , and liquid bridge axial length  $L$ ) of the setup. (f) Illustration of stretched macromolecules and the corresponding length scale, the contour length  $L_c$ .



Detailed calculations are included in the SI [99]. The concentration range of depletion suspensions was  $0.3 < c/c^* < 2.5$  for USP and ULP and  $0.2 < c/c^* < 0.7$  for DP. We extended the range of concentrations for USP and ULP polymers to understand the effect of polymer size decoupled from dispersity.

## B. Confocal microscopy

We examined the quiescent structure of particle suspensions by using confocal microscopy. The microscopy setup consisted of a Leica SP8 confocal system and a Leica DMi 8 microscope (Leica Microsystems, Buffalo Grove, IL) with a  $63\times$  oil-immersion objective (numerical aperture of 1.4). To characterize the 3D structure of the suspensions, we acquired a series of 2D images with a vertical spacing of  $\Delta z = 0.1 - 0.3 \mu\text{m}$  between images from  $z = 25$  to  $65 \mu\text{m}$  above the bottom of the sample chamber and located the particle positions in 3D using algorithms written in IDL (Interactive Data Language) [72].

To partially screen the electrostatic repulsion and achieve nearly hard-sphere interparticle interactions between the particles, we added NaCl to all suspensions. To determine the salt concentration at which the interparticle interactions were nearly hard-sphere, we imaged dilute ( $\phi = 0.01$ ) suspensions at salt concentrations ranging from 0 to 20 mM. By calculating the pair-correlation function  $g(r)$  and interaction potential  $u/kT$ , we determined that a salt concentration of 1.5 mM produced nearly hard-sphere interactions (Fig. S1) [99]. For suspensions containing polymer that formed gels, we estimated the correlation length  $\xi$  associated with the depletion gel network (Fig. S2) [99] by calculating the number density fluctuations (Fig. S3) [99].

## C. Shear rheology

We measured the viscosity and first normal stress difference using a DHR-2 rheometer (TA Instruments, New Castle, DE) equipped with a 40 mm diameter  $2^\circ$  cone-plate hard-anodized aluminum geometry and using a  $59 \mu\text{m}$  gap. Before each measurement, all samples were treated with a consistent preshear protocol [65]. Briefly, samples were sheared as the rate was increased from  $0.5$  to  $50 \text{ s}^{-1}$  for 30 s, at  $50 \text{ s}^{-1}$  for 30 s, and then allowed to rest for 300 s. After preshear, we carried out a forward flow sweep from  $0.1$  to  $800 \text{ s}^{-1}$  and a backward flow sweep from  $800$  to  $0.1 \text{ s}^{-1}$  with six shear rates per decade. Below  $100 \text{ s}^{-1}$ , samples were equilibrated for 30 s and averaged for 10 s. Above  $100 \text{ s}^{-1}$ , samples were equilibrated for 5 s and averaged for 5 s. All

**TABLE II.** Polyacrylamide properties.

Parameter	USP	ULP	DP
$M_w$ (kDa)	194	1000	1970
$\mathcal{D}$	1.24	1.25	21
$c^*$ (mg mL $^{-1}$ )	12	3.2	5.1
$R_g$ (nm)	19	50	75
$R_{us}$ (nm)	47	122	184
$L_c$ (nm)	842	4338	8546

normal stress measurements were corrected by subtracting the inertial contributions [73] and the initial value at the lowest shear rate. The Péclet number  $Pe = t_B \dot{\gamma}$  in the shear experiments for all depletion suspensions ranged from  $1.8 \times 10^1 < Pe < 1.1 \times 10^6$ , indicating that convection dominates over diffusion.

## D. Extensional rheology

The dripping-onto-substrate (DoS) setup was based on that used in [74,75] with several modifications [Figs. 1(d) and 1(e)]. A custom-machined stage was attached to a laboratory jack by bolt and screw. On the stage was mounted a needle holder with adjustable height that was angled toward the stage. A 2 in. 18G (1.27 mm O.D.) blunt tip needle and a syringe pump (Chemyx Fusion 200) were used to create the liquid bridge. We used the same DoS setup for the depletion suspensions as for the polymer solutions because the nozzle radius  $R_0$  is  $O(10^3)$  larger than the particle radius. We imaged the pinching dynamics with a high-speed camera (Chronos 1.4, KronTech) at 8819.12–15 676.4 frames per second and processed the images using algorithms written in MATLAB [63] to obtain the time evolution of the filament diameter during pinching. The image resolution at these frame rates was estimated from the needle O.D. to be  $\approx 6 - 7 \mu\text{m}$ . The captured image had a matrix size of  $240 \times 640 \text{ pixels}^2$  for 8819.12 fps and  $216 \times 384 \text{ pixels}^2$  for 15 676.4 fps, which gives a physical field of view of width  $1.3 - 1.7 \mu\text{m}$  and height  $2.3 - 4.5 \mu\text{m}$ . In the image processing algorithm, we performed a hole-filling morphological transform on the image to remove irrelevant features and detected the diameter of the filament by implementing a subpixel edge detection algorithm [76]. The length scales involved in this experiment are summarized in Table III.

## E. DoS analysis

To fit the  $R(t)$  data, we considered the time evolution of the radius for different types of fluids. In a Newtonian fluid, the time evolution of the filament radius is determined by the contribution of viscous forces in capillary-driven breakup, estimated from the Ohnesorge number  $Oh = \eta_0 / (\rho \sigma R_0)^{1/2}$ , the ratio of viscous to inertial and surface tension forces. The radius of a viscous Newtonian fluid ( $Oh > 1$ ) decays linearly

**TABLE III.** Length scales of dripping-onto-substrate setup, particle suspension, and polymer.

<i>DoS setup</i>		
$R_0$ (mm)	Nozzle outer radius	0.635
$H_0$ (mm)	Distance from nozzle to substrate	3.8
$L$ (mm)	Axial liquid bridge length	0.3–0.8
<i>Particle suspension</i>		
$a$ ( $\mu\text{m}$ )	Particle radius	0.90
$h$ ( $\mu\text{m}$ )	Interparticle spacing	0.41
$\xi$ ( $\mu\text{m}$ )	Correlation length	14–21
<i>Polymer</i>		
$R_g$ (nm)	Radius of gyration	19–75
$R_{us}$ (nm)	Unstretched polymer length	47–184
$L_c$ ( $\mu\text{m}$ )	Contour length	0.84–8.5

with time according to the viscopillary (VC) response [24,77,78],

$$\frac{R(t)}{R_0} = \frac{(2X_{vc} - 1)}{6} \left( \frac{\sigma}{\eta_0 R_0} \right) (t_f - t), \quad (2)$$

where  $\sigma$  is the surface tension,  $\eta_0$  is the zero-shear viscosity,  $R_0$  is the nozzle radius,  $X$  is a numerical prefactor [79] of  $O(1)$  [80], and  $t_f$  is the total filament lifespan. Below  $Oh < 1$ , the time evolution of the radius enters the inertio-capillary (IC) regime and exhibits a power-law decay with an exponent of  $2/3$  [78,81,82],

$$\frac{R(t)}{R_0} = X_{ic} \left( \frac{\sigma}{\rho R_0^3} \right)^{1/3} (t_f - t)^{2/3}, \quad (3)$$

where  $\rho$  is the fluid density and  $X_{ic}$  is a  $O(1)$  numerical prefactor.

The filament radius of a non-Newtonian shear-thinning fluid follows a power-law (PL) decay [75,78],

$$\frac{R(t)}{R_0} = Y(t_f - t)^{n_e}, \quad (4)$$

where  $n_e$  is the extensional power-law exponent and  $Y$  is a constant that depends on material properties. Finally, the radius evolution for a solution of polymers in a Newtonian solvent initially exhibits a Newtonian scaling regime and then follows an exponential decay with time [83]. The latter regime can be described by the elastocapillary (EC) equation [24,84],

$$\frac{R(t)}{R_0} = \left( \frac{G_E R_0}{2\sigma} \right)^{1/3} \exp[-(t - t_c)/3\lambda_E], \quad (5)$$

where  $G_E$  is the elastic modulus and  $t_c$  is the transition time from Newtonian to EC response at the transition radius  $R_c \approx R_0(G_E R_0/2\sigma)^{1/3}$ . As the polymer molecules reach their fully stretched length, however, the radius evolution transitions back to a linear decay due to the finite extensibility

**TABLE IV.** Time scales for particle diffusion, bond formation, and polymer extensional relaxation in the pinching dynamics of colloid-polymer mixtures. The values are provided for polymer concentrations  $0.3 < c/c^* < 2.6$  for USP and ULP and  $0.2 < c/c^* < 0.7$  for DP.

Diffusive time scales (s)				
Length scale	NP	USP	ULP	DP
$a$	180		240–1500	
$h$	40		50–300	
$R_g$	—	0.11–0.68	0.73–4.7	1.7–11
Bond formation time scale (s)				
$2R_g$	—	1.4–9.1	9.8–63	22–140
Polymer extensional relaxation time (ms)				
—	—	0.39–1.0	3.1–12	2.5–12

effect [24,83],

$$\frac{R(t)}{R_0} = \left( \frac{\sigma}{2R_0\eta_{E,\infty}} \right) (t_f - t), \quad (6)$$

where  $\eta_{E,\infty}$  is the terminal steady-state extensional viscosity, in the terminal viscoelastocapillary (TVEC) regime. The fitting routine is included in [63]. We adopted continuum analyses for the pinching dynamics of the colloid-polymer mixtures following previous studies of noncolloidal suspensions in Newtonian [37] and viscoelastic [44] media.

When the filament radius in capillary-driven pinching reaches a self-similar shape, we can estimate the extensional viscosity by balancing the capillary force and the viscous and elastic fluid forces,

$$\eta_E = \frac{\sigma}{\dot{\epsilon}R(t)}, \quad (7)$$

where the strain rate  $\dot{\epsilon}$  can be estimated from the time derivative of the radius evolution,

$$\dot{\epsilon} = -\frac{2}{R} \frac{dR}{dt}. \quad (8)$$

## F. Suspension and solution time scales

The time scales for particle diffusion are calculated using  $t_D = l^2/D$ , where  $l$  is a suspension lengthscale (the particle radius  $a$ , interparticle spacing  $h$ , and polymer radius of gyration  $R_g$ ) and  $D = k_B T / 6a\pi\eta_m$  is the diffusion coefficient of the particles in a medium of viscosity  $\eta_m$ . The diffusion coefficient for particles in the glycerol-water solvent is  $D = 4.3 \times 10^{-15} \text{ m}^2 \text{ s}^{-1}$ .

The bond formation time scale is estimated as  $t_{\text{bond}} = (2R_g)^2/D_s^s$ , where  $D_s^s$  is the short-time self-diffusivity of the particles [85]. For  $\phi = 0.40$  suspensions,  $D_s^s \approx 0.3D$  [86]. Table IV presents the diffusive and bond formation time scales as well as the polymer extensional relaxation times  $\lambda_E$  of PAM in 80% (w/w) glycerol-water solvent ( $\eta_s = 0.056 \text{ Pa} \cdot \text{s}$ ) from [63].

During pinching, the strain rate experienced by the fluid  $\dot{\epsilon}$  decreases with viscosity and increases with time [Eq. (8)]. We estimated the Péclet number during pinching from  $\text{Pe}_{\text{ext}} = \dot{\epsilon}t_B$ , where  $t_B$  is the Brownian time scale [43], which corresponds to the diffusive time scale with  $l = a$  in Table IV. In our experiments,  $\text{Pe}_{\text{ext}}$  ranges from  $6.0 \times 10^3$  to  $3.8 \times 10^6$ .

## III. RESULTS AND DISCUSSION

### A. Shear rheology

We first characterize the steady shear viscosity of colloid-polymer depletion suspensions. The shear viscosity of USP suspensions with constant  $\phi = 0.40$  increases with polymer concentration and is nearly independent of shear stress  $\sigma$ , increasing only slightly at high  $\sigma$  [Fig. 2(a)]. By contrast, both ULP and DP suspensions exhibit shear thinning at low  $\sigma$  and modest shear thickening at high  $\sigma$ , which, respectively,

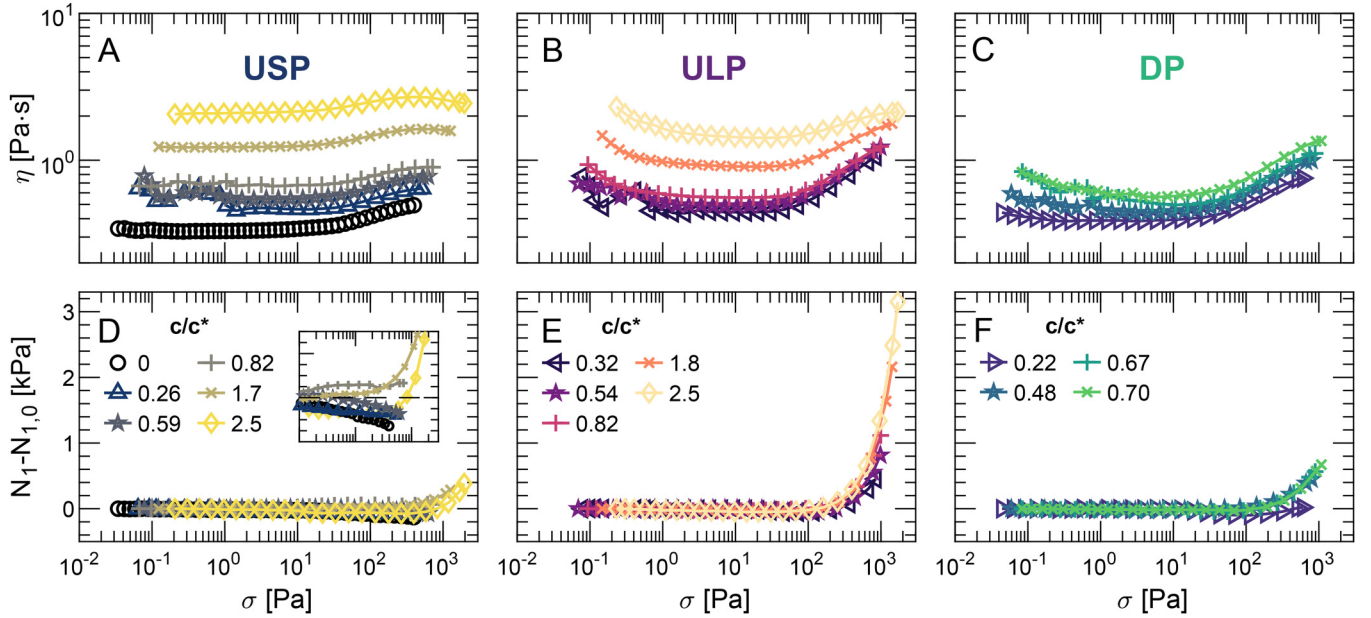


**FIG. 2.** Shear rheology of depletion suspensions with  $\phi = 0.40$  and (a) and (d) USP, (b) and (e) ULP, and (c) and (f) DP polymers at various free volume concentrations  $c/c^*$  in 80 (w/w)% glycerol/water with 1.5 mM NaCl. (a)–(c) Viscosity  $\eta$  and (d)–(f) the first normal stress difference  $N_1 - N_{1,0}$  as a function of shear stress  $\sigma$ . (d) Inset:  $N_1 - N_{1,0}$  at  $\sigma > 10$  Pa shows negative values for  $c/c^* = 0 - 0.59$  and positive values for  $c/c^* = 0.82 - 2.5$ . The horizontal dashed lines represent  $N_1 - N_{1,0} = 0$  kPa.

strengthen and weaken upon increasing  $c/c^*$  [Figs. 2(b) and 2(c)]. The ULP and DP suspensions that exhibit shear thinning at low  $\sigma$  contain interconnected networks of particles under quiescent conditions, as determined using confocal microscopy; by contrast, particles in USP suspensions remain primarily dispersed, independent of polymer concentration (Fig. S2) [99]. Thus, the size and dispersity of the polymer affect the shear rheology response of colloid-polymer depletion suspensions, in accord with our previous study [64].

The first normal stress difference  $N_1$  also depends on polymer size and dispersity. A colloidal particle suspension with no added polymer ( $c/c^* = 0$ ) exhibits a negative  $N_1 < 0$  at high  $\sigma$ , as expected for dense hard-sphere suspensions [87–89] and attributed to thickening driven by hydrodynamic forces [88,89]. For suspensions containing USP,  $N_1$  switches sign from negative to positive at high  $\sigma$  as  $c/c^*$  is increased [Fig. 2(d), inset]. For ULP and DP suspensions, by contrast,  $N_1$  at high  $\sigma$  is positive for all polymer concentrations studied and increases with  $c/c^*$  [Figs. 2(e) and 2(f)]. In colloidal suspensions, positive values of  $N_1$  accompanied by shear thickening are typically attributed to the formation of a contact network of particles [88]. In our previous study, we attributed the positive  $N_1$  values to size-dependent exclusion of large polymers from the fluid layers between the colloids, which promoted particle-particle contacts [64]. We suggest that the stronger shear thickening in ULP and DP suspensions in these experiments is also driven by contacts between particles through exclusion of large polymers.

In the semidilute regime ( $c > c^*$ ), the shear-thickening response appears to be obscured by the increase in viscosity at low  $\sigma$ , despite the increase in  $N_1$ . This result is consistent with an earlier study on depletion mixtures of silica particles and polystyrene [90], which found that the shear-thickening

contributions of the particles are masked by the increase in viscosity and/or shear-thinning response from the addition of polymer. In our systems, the strongest increase in suspension viscosity occurs for the mixtures that contain the smallest polymers (USP). Thus, polymer size affects the concentration-dependent viscosity as well as the shear thickening and first normal stress difference.

## B. Extensional rheology of solvent, polymer solutions, and colloidal suspension without polymer

We determine the extensional rheology from the analysis of change in radius with time of a liquid neck undergoing pinching [Figs. 3(a) and 3(b)]. The shape of the neck and its pinching dynamics during thinning can provide insight into the time-dependent extensional viscosity and the physics controlling capillary breakup [24]. Images of the time-dependent evolution of the neck radius reveal differences between the 80 (w/w)% glycerol/water solvent, a dilute solution of USP PAM with  $c/c^* = 0.4$ , and a colloidal suspension with particle volume fraction  $\phi = 0.40$  [Figs. 3(c)–3(f)]. The glycerol/water solvent exhibits the pinching dynamics of a viscous Newtonian fluid: the neck is initially strongly curved and gradually evolves to a self-similar cylindrical shape before pinch-off [Fig. 3(c)]. A cylindrical neck is also associated with elastic or weakly elastic fluids and for power law fluids if the exponent is close to one [24,75,78]. Adding polymers or particles increases the time for filament breakup. In the PAM solution, the transition to a cylindrical neck shape occurs at a larger neck diameter [Figs. 3(d)–3(e)] due to PAM elasticity. In the dense colloidal suspension, by contrast, the final neck shape is biconical with a minimum in width at the

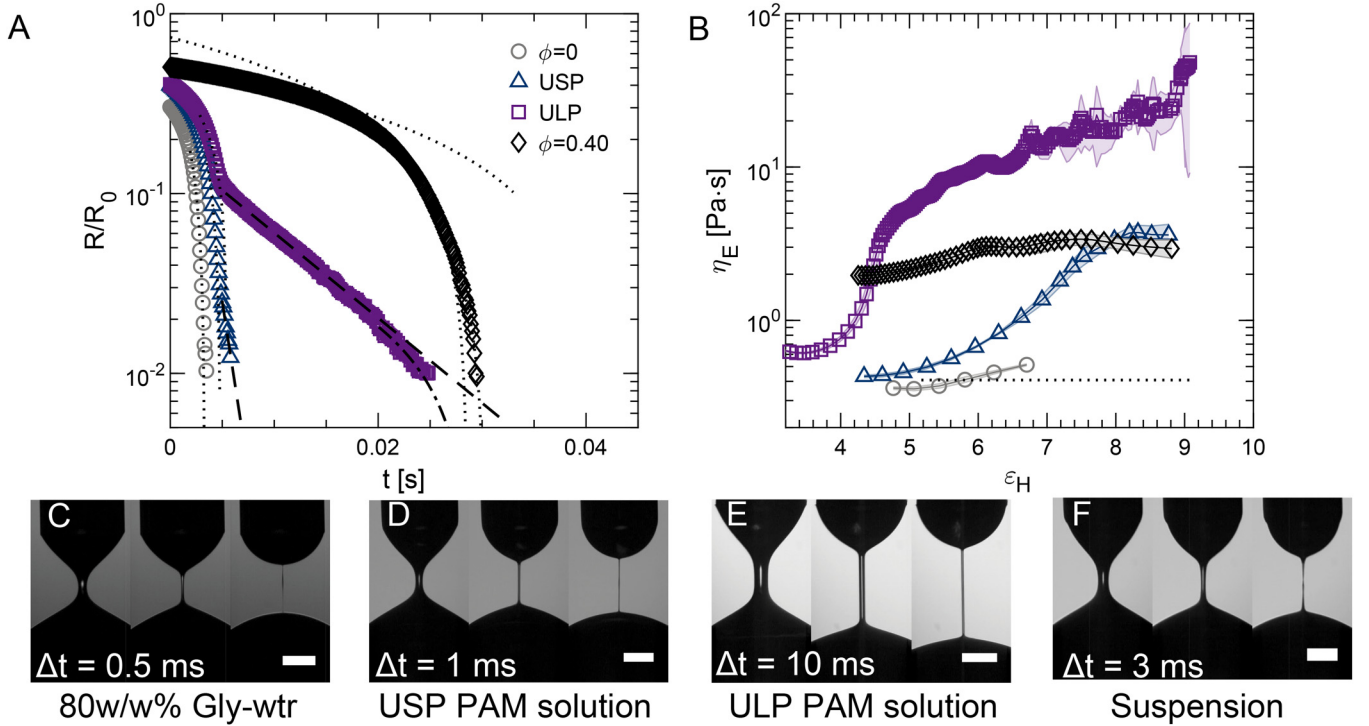


**FIG. 3.** Pinching dynamics and extensional rheology of complex fluids. (a) Time evolution of the normalized filament radius  $R/R_0$  of background solvent of 80 (w/w)% glycerol/water, of USP and ULP polyacrylamide solutions, and of a colloidal suspension with  $\phi = 0.40$ . Dashed lines show elastocapillary fitting and dotted lines show viscocapillary fitting for USP and power-law fitting for ULP. The normalized polymer concentration in the USP and ULP samples is  $c/c^* \approx 0.26$ . (b) Extensional viscosity calculated from (a) as a function of Hencky strain  $\epsilon_H$ . Errors are calculated from the standard deviation from multiple replicates and represented as shaded area. Data for polymer solutions without particles are taken from [63]. (c)–(f) Snapshots of pinch-off dynamics of (c) the Newtonian 80 (w/w)% glycerol/water solvent, (d) a  $0.4c/c^*$  USP polyacrylamide (PAM) solution, (e) a  $0.4c/c^*$  USP polyacrylamide (PAM) solution, and (f) a  $\phi = 0.40$  TtMA colloidal suspension in 80 (w/w)% glycerol/water. Scale bars are 0.5 mm.

center [Fig. 3(f)]. This neck shape is commonly associated with power-law and yield stress fluids [24,75,78,91–93].

The filament radius of the glycerol/water background solvent decays approximately linearly with time, indicative of VC scaling [Fig. 3(a) and Eq. (2)] even though  $Oh = 0.25$  for our glycerol/water solvent. The solvent exhibits VC scaling because viscous forces dominate at smaller length scales approaching the Ohnesorge unit length  $l_{Oh} = \eta^2/(\sigma\rho)$ , which is  $l_{Oh} = 38 \mu\text{m}$  in our glycerol/water mixture.

The radius evolution of USP and ULP solutions, by contrast, exhibits a PL scaling regime [Eq. (4)] on short time scales and transitions to EC scaling [Eq. (5)] on long time scales. A similar PL to EC transition was observed in DoS rheometry studies that analyzed pinching dynamics of entangled aqueous polysaccharide solutions [94]. The scaling exponents in the PL regime are  $n_e \approx 1$  for USP and  $n_e \approx 0.7$  for ULP. When the neck radius is normalized by  $l_{Oh}$  (Fig. S4) [99], we observe that the PL scaling regime for ULP lies above the line  $R/l_{Oh} = Oh^{-2} > 1$ , suggesting that the PL scaling exponent in ULP represents an inertia-dominated regime. The radius at the transition depends on the polymer size and the elasticity of the dispersion [Fig. 3(a)]. The USP solution transitions to the EC regime at  $R/R_0 \approx 0.03$ , whereas the ULP solution transitions at  $R/R_0 \approx 0.1$ . Thus, the duration of the EC regime is much shorter in USP than in ULP. This result suggests that ULP is much more extensible than USP, consistent with molecular weight and dispersity and our prior study [63]. Prior to

pinch-off, we observe a deviation from the EC scaling in ULP that can be fit with the TVEC equation. Although both polymer solutions are expected to reach a TVEC regime due to the finite extensibility effect, our experimental resolution is not sufficient to capture this regime for small polymers such as USP.

In dense colloidal suspensions ( $\phi = 0.40$ ), the radius time evolution cannot be fit with a single PL equation. Instead, the radius evolution exhibits three distinct regimes, which we fit with three power-law equations [Eq. (4) and Fig. S5]. The dynamics accelerate from the first to the second regime and decelerate from the second to the third. All three fits yield exponents that are close to 1, indicating that viscous forces dominate the pinch-off process. Because the scaling is linear, we associate  $Y$  with the prefactor from the VC scaling in Eq. (2), where  $Y \sim 1/\eta_0$ . The distinct fits indicate that the effective viscosity of the suspension varies with filament radius. We examine only the second and third viscocapillary regimes, as the first viscocapillary fit may be affected by a mixed flow profile. The slight increase in  $\eta_E$  may correlate with the slight shear thickening response for this suspension [Fig. 2(a)].

The extensional viscosity profiles of the Newtonian solvent, the USP and ULP solutions, and the  $\phi = 0.40$  suspension exhibit distinct dependencies on the Hencky strain  $\epsilon_H = 2 \ln(R_0/R(t))$  [Fig. 3(b)]. In a Newtonian fluid,  $\eta_E$  is expected to be constant after the neck reaches a self-similar shape. For 80 (w/w)% glycerol/water, however,  $\eta_E$  increases



for  $\varepsilon_H > 6$ . This deviation from the expected behavior may be due to the limited resolution of the captured neck diameter right before pinch-off: the last three data points representing the radius of 80 (w/w)% glycerol/water deviate from the VC scaling [Fig. 3(a)], which would manifest as an unphysical increase in  $\eta_E$ . For USP and ULP solutions,  $\eta_E$  increases with  $\varepsilon_H$ . The increase in  $\eta_E$  corresponds to strain hardening that occurs as polymer chains get stretched and aligned in the strong extensional flow created by the capillarity-driven squeeze flow in the neck. The interplay of  $c$  and polymer contribution to viscoelastic stresses within the fluid neck leads to the exponential decay in the EC regime. The increase in  $\eta_E$  is much larger in ULP than in USP because the start and duration of the EC regime are longer for ULP than for USP. In ULP,  $\eta_E$  at the highest  $\varepsilon_H$  is in good agreement with the  $\eta_{E,\infty}$  obtained from TVEC scaling, indicating that the TVEC scaling represents the physics just prior to pinch-off in ULP solutions. Finally,  $\eta_E$  for the dense suspension is nearly independent of  $\varepsilon_H$  as the pinching radius follows VC scaling.

### C. Comparing radius evolution and extensional viscosity

To understand the effect of adding particles on the pinching dynamics and extensional rheology response, we first compare the pinching dynamics of depletion suspensions to those of polymer solutions at similar free volume polymer concentration (Fig. 4). For all three polymers (USP, ULP, and DP), the addition of particles increases the total filament lifetime by increasing the duration of the PL scaling regime [described by Eq. (4)]. Although the transition to EC scaling occurs at a smaller normalized neck radius, the decay rate in the EC scaling regime [Eq. (5)] is similar for the polymer solution and depletion suspension.

On longer time scales before pinch-off, we compare the neck shape and radius evolution between particle suspensions with and without polymer additives (Fig. 5). Although all depletion suspensions exhibit an EC regime that is comparable to that in a polymer solution at similar free volume concentration (Fig. 4), the neck shapes of the suspensions with USP are surprisingly different from those of USP solutions. The neck shape of the USP PAM [Fig. 5(a)], like that of the colloidal suspension without polymer, is biconical. Thus, addition of USP does not strongly affect the pinch-off shape compared to the no-polymer suspension [Figs. 5(c) and 5(d)] but instead leads to an exponential decay scaling of  $R(t)$  before pinch-off. In ULP and DP suspensions, by contrast, the liquid neck bridge is cylindrical in the EC regime [Fig. 5(b)], as also observed for the corresponding polymer solutions.

Furthermore, right before pinch-off, the scaling of the radius evolution for the ULP and DP suspensions departs from the EC scaling and pinching slows down. This behavior is different than the pinch-off response of a polymer solution, where the EC scaling regime is followed by the TVEC scaling regime with faster pinching of the neck regime due to the finite extensibility effect. We posit that the presence of particles at a moderately high concentration ( $\phi = 0.40$ ) contributes to this scaling response. By contrast, nail lacquer formulations exhibited PL to TVEC scaling, attributed to presence of nitrocellulose as a polymer additive to a complex fluid with a lower particle concentration (maximum  $\sim 15$  wt. %) [7].

Increasing the polymer concentration in colloidal suspensions slows the pinching (Fig. 6). In USP suspensions, this slowing occurs gradually [Fig. 6(a)]. The radius evolution follows a PL scaling that transitions to EC scaling near pinch-off ( $R/R_0 \approx 0.02$ ), indicating that PL scaling

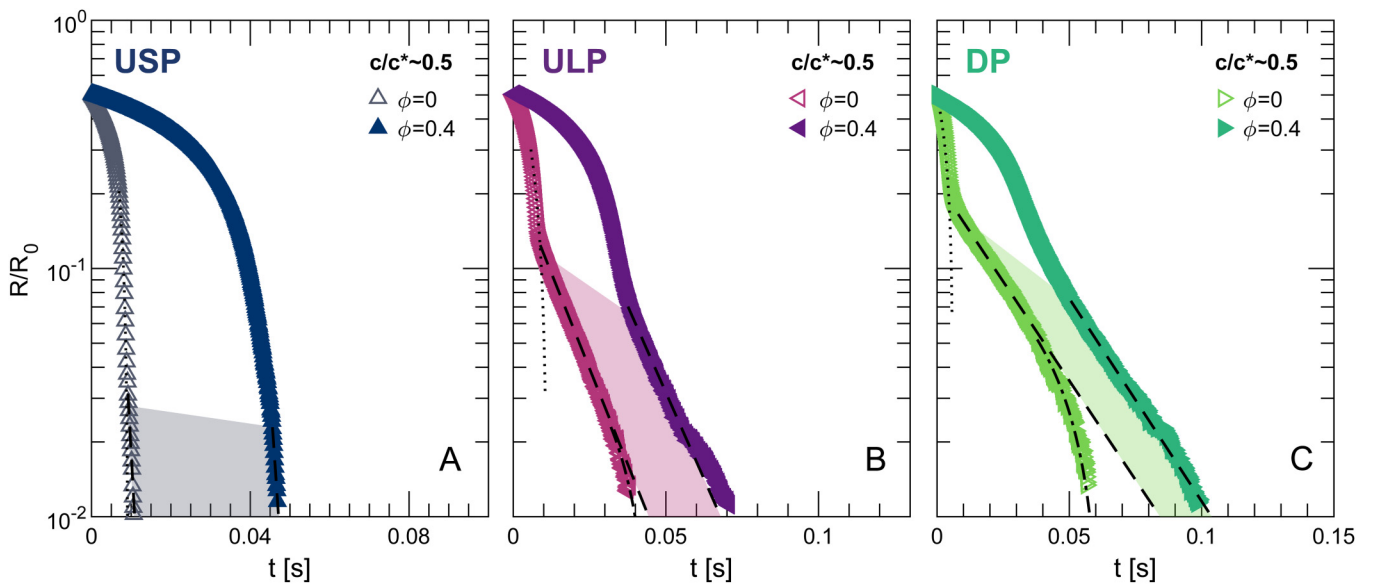


**FIG. 4.** Pinching dynamics of (a) USP, (b) ULP, and (c) DP of polymer solutions  $\phi = 0$  and depletion suspensions at particle volume fraction  $\phi = 0.40$  at similar free volume polymer concentrations  $c/c^* \approx 0.5$  in 80 (w/w)% glycerol/water with 1.5 mM NaCl, determined as the time evolution of the normalized radius  $R/R_0$ . The time  $t = 0$  is defined at  $R/R_0 = 0.50$ , as the early stages of the radius evolution are sensitive to variability arising from substrate wettability and deformation history within the nozzle. Dotted lines indicate PL fitting [Eq. (4)], dashed lines indicate EC fitting [Eq. (5)], and dotted-dashed lines indicate TVEC fitting [Eq. (6)]. The shaded area represents a visual aid to illustrate the similarity in exponential decay-rate between  $\phi = 0$  and  $\phi = 0.40$ .

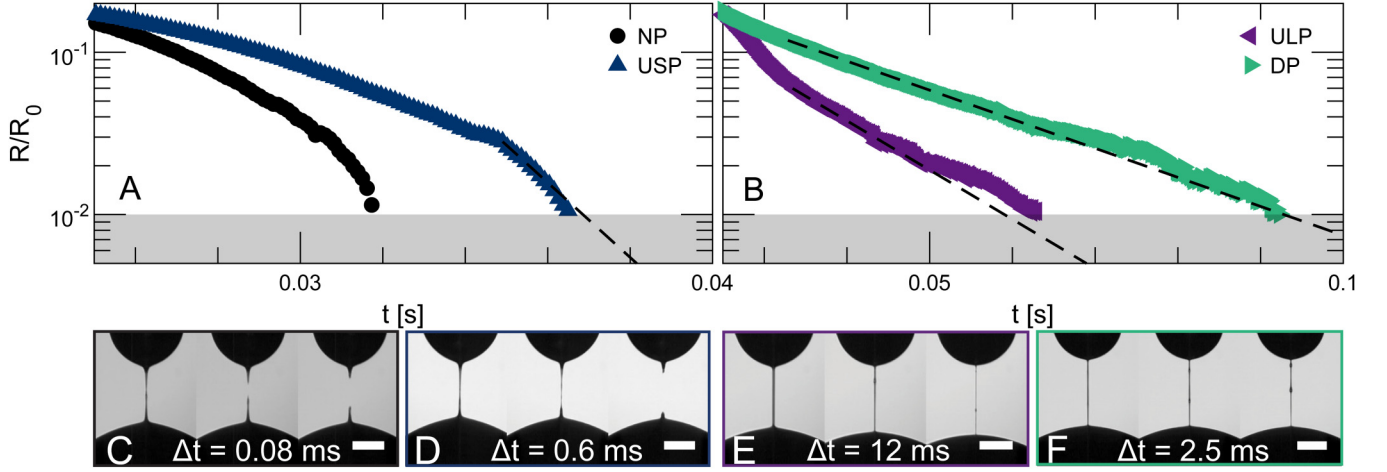


**FIG. 5.** Time evolution of the normalized radius  $R/R_0$  of  $\phi = 0.40$  suspensions in 80 (w/w)% glycerol/water with 1.5 mM NaCl (a) without polymer (NP) and with USP polyacrylamide (PAM) and (b) with ULP and DP PAM. The free volume concentration of the polymer solutions is  $c/c^* \approx 0.5$ . Dashed lines indicate EC fitting [Eq. (5)]. The gray shaded area indicates the spatial resolution limit of  $R/R_0 = 0.01$ . The scale bars are 0.5 mm. (c)–(f) Snapshots of the pinch dynamics of  $\phi = 0.40$  suspensions (c) without polymer and with (d) USP, (e) ULP, and (f) DP at  $c/c^* \approx 0.5$ .

dominates within the overall radius evolution of USP suspensions. ULP suspensions also exhibit a transition from PL to EC scaling in the radius evolution, but the transition to EC scaling starts earlier at  $R/R_0 \approx 0.07$  [Fig. 6(b)]. The transition from PL to EC in USP and ULP suspensions occurs slightly later (i.e., on longer times and at smaller neck diameters) compared to USP and ULP solutions without particles [Fig. 3(a)]. DP suspensions with increasing polymer concentration also exhibit a later transition to the EC regime, compared to the corresponding DP solution, at  $R/R_0 \approx 0.1$  [Fig. 6(c)]. Both the transition radius  $R_c$  and the EC duration  $\Delta t_{EC}$  increase with polymer  $M_w$ , following USP < ULP < DP.

The increase in the time required for the liquid bridge to break with polymer concentration may arise from the increase

in either viscous (indicated by duration of PL regime  $\Delta t_{PL}$ ) or elastic (indicated by  $\Delta t_{EC}$ ) forces of the suspensions [83,95]. In USP suspensions, the increase in bulk viscosity controls the polymer contributions as PL scaling dominates the radius evolution. In ULP and DP suspensions, the viscous and elastic contributions are approximately equal at low concentration and the elastic force dominates at higher polymer concentration.

Notably, the quiescent microstructure of the depletion suspensions (Fig. S2) [99] does not qualitatively alter the pinching dynamics, as can be seen by comparing DP suspensions at  $c/c^* = 0.22$  and at higher  $c/c^*$ . Confocal micrographs reveal that the DP suspension at  $c/c^* = 0.22$  does not form a network (Fig. S2, panel D1) [99], whereas those with greater  $c/c^*$  do (Fig. S2, panels D2 and D3) [99]. Nevertheless, the

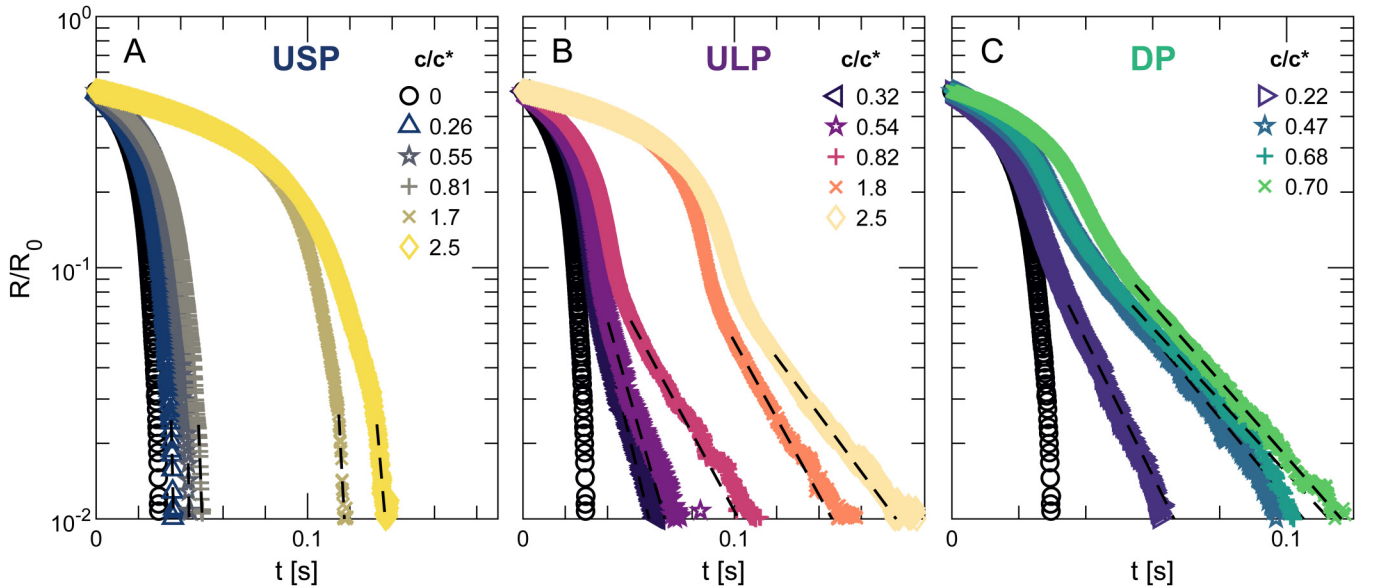


**FIG. 6.** Pinching dynamics of (a) USP, (b) ULP, and (c) DP depletion suspensions at particle volume fraction  $\phi = 0.40$  in 80 (w/w)% glycerol/water with 1.5 mM NaCl, determined as the time evolution of the normalized radius  $R/R_0$ . The time  $t = 0$  is defined at  $R/R_0 = 0.50$ , as the early stages of the radius evolution are sensitive to variability arising from substrate wettability and deformation history within the nozzle. Dashed lines indicate EC fitting [Eq. (5)].

pinching dynamics for all DP suspensions follow a PL to EC transition.

To investigate the role of polymer on the resistance of depletion suspensions to stretching, we calculate  $\eta_E(\varepsilon_H)$  of the suspensions (Fig. 7). We evaluate  $\eta_E$  starting from  $\varepsilon_H \approx 4$ , which corresponds to  $R/R_0 \approx 0.1$  where the neck morphology approaches a self-similar shape, and define the initial extensional viscosity  $\eta_{E,0} = \eta_E(\varepsilon_H \approx 4)$ . In USP suspensions,  $\eta_E$  increases with  $\varepsilon_H$  by less than an order of magnitude [Fig. 7(a)]. Although increasing the polymer concentration gradually increases  $\eta_{E,0}$ , the extent of extensional thickening with  $\varepsilon_H$  varies by less than an order of magnitude with polymer concentration. In ULP suspensions, by contrast,  $\eta_E$  increases by an order of magnitude with  $\varepsilon_H$ , and increasing the polymer concentration leads to marked increases in both  $\eta_{E,0}$  and the extent of extensional thickening [Fig. 7(b)]. The DP suspensions behave similarly to ULP suspensions [Fig. 7(c)].

For the colloid-polymer suspensions,  $\eta_{E,0}$  is close to  $7\eta_0$ , the theoretical prediction for viscous Newtonian systems based on viscocapillary scaling with a prefactor of  $(2X_{vc} - 1)/6 = 0.0709$  [77]. This trend is consistent across all depletion suspensions, suggesting that the calculated  $\eta_{E,0}$  represents the viscous response under extensional flow. The elastic response manifests in the increase in  $\eta_E$  with  $\varepsilon_H$ , and the extent of this extensional thickening increases with polymer  $M_w$ . This result is consistent with the different scaling regimes for the radius evolution (Fig. 6): USP suspensions, for which the extensional flow mostly follows PL scaling, thicken modestly in extension compared to ULP and DP suspensions, which exhibit both PL and EC scaling regimes of approximately equal duration in time.

The steady-state Trouton ratio  $\text{Tr}^\infty = \eta_{E,\infty}/\eta_0$  is a measure of the relative importance of extensional and shear rheological properties [96] and the degree of stretching of the fluids. Here,  $\eta_{E,\infty}$  is determined at the highest measured  $\varepsilon_H$  (Figs. S6–S7) [99] and  $\eta_0$  is determined at the plateau at intermediate shear stress (Figs. 2, S8). For USP,  $\text{Tr}^\infty \approx 8$ –14,

whereas for ULP and DP,  $\text{Tr}^\infty \approx 80$ –140. The Trouton ratio for USP suspensions is similar to that obtained for pinch-off of nail lacquers containing particles and polymers (estimated  $M_w = 100$ – $300 \text{ kg mol}^{-1}$ ),  $\text{Tr}^\infty \approx 7$ – $15$  [7]. For polymer solutions in a similar  $c/c^*$  range,  $\text{Tr}^\infty \approx 20$ – $60$  for USP and  $\text{Tr}^\infty \approx 180$ – $440$  for ULP and DP. Thus, the presence of particles reduces the magnitude of  $\text{Tr}^\infty$  (Fig. S9) [99], suggesting that particles affect the degree of stretching of the fluids.

## D. Comparing relaxation and filament time scales

To elucidate the contribution of polymer additives on the extensional flow, we compare the material properties of the depletion suspensions and polymer solutions without any particles. First, we examine the extensional relaxation time  $\lambda_E$ , which characterizes the elastic response manifesting as an exponential decay in the radius evolution plots (Fig. 6) and is determined using Eq. (5). The  $\lambda_E$  values for both polymer solutions and depletion suspensions collapse onto scaling curves as a function of  $c/c^*$  [Figs. 8(a)–8(c)]. The collapse indicates that the elastic response in both solutions and suspensions is controlled by the free volume polymer concentration. A similar response was found for mixtures of noncolloidal polystyrene particles and poly(ethylene oxide) polymers, where the concentration and molecular weight of the polymers were held constant [44]. For those PS-PEO systems, the characteristic time scale corresponding to  $\lambda_E$  was constant for suspensions containing particles of various sizes and volume fractions. In our experiments, the scaling exponents in the dilute regime ( $c < c^*$ ) differ for the three polymers and follow the polymer macromolecular properties, consistent with prior studies [62,63]. Our results, thus, suggest that the polymer pinch-off response controls the elastic response in depletion suspensions.

To understand the viscous contributions from the polymers, we compare the filament lifespan  $t_f$  of the polymer solutions and the depletion suspensions. The lifespan  $t_f$  is a practically relevant time scale that includes the duration of

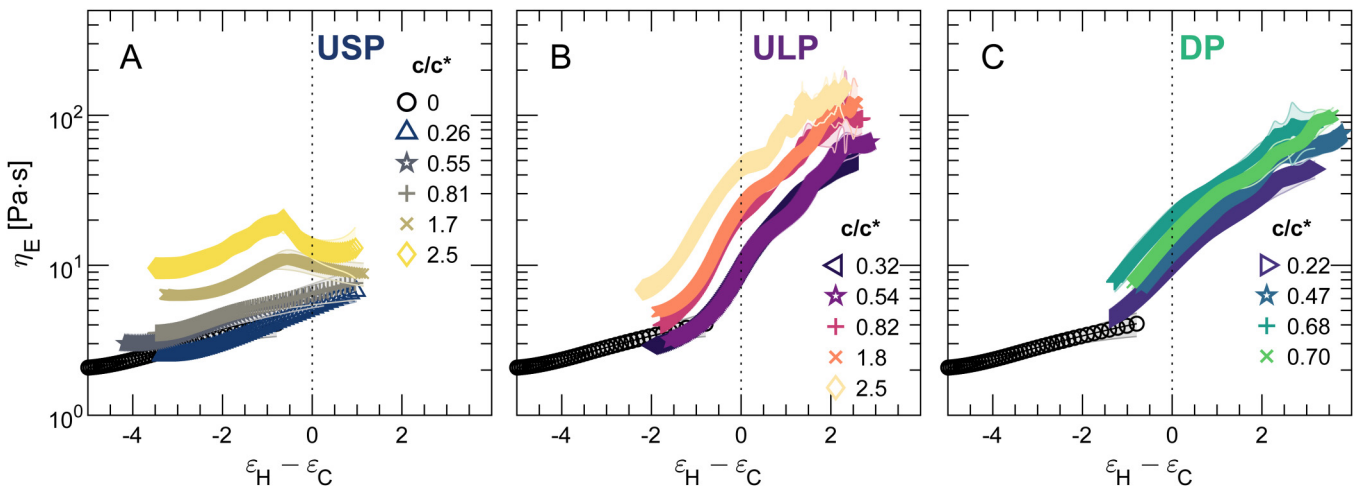


**FIG. 7.** Extensional viscosity  $\eta_E$  as a function of Hencky strain  $\varepsilon_H$  shifted by transition Hencky strain  $\varepsilon_C$ , which represents the elastocapillary transition, for  $\phi = 0.40$  depletion suspensions with (a) USP, (b) ULP, and (c) DP depletants in 80 (w/w)% glycerol/water with 1.5 mM NaCl. (For  $\phi = 0.40$ , without polymer, which does not exhibit an EC regime,  $\varepsilon_C$  is chosen to be 9.2, and the value of  $\varepsilon_H$  at  $R/R_0 = 0.01$ .) Errors are calculated from the standard deviation of replicate measurements and represented as shaded areas.

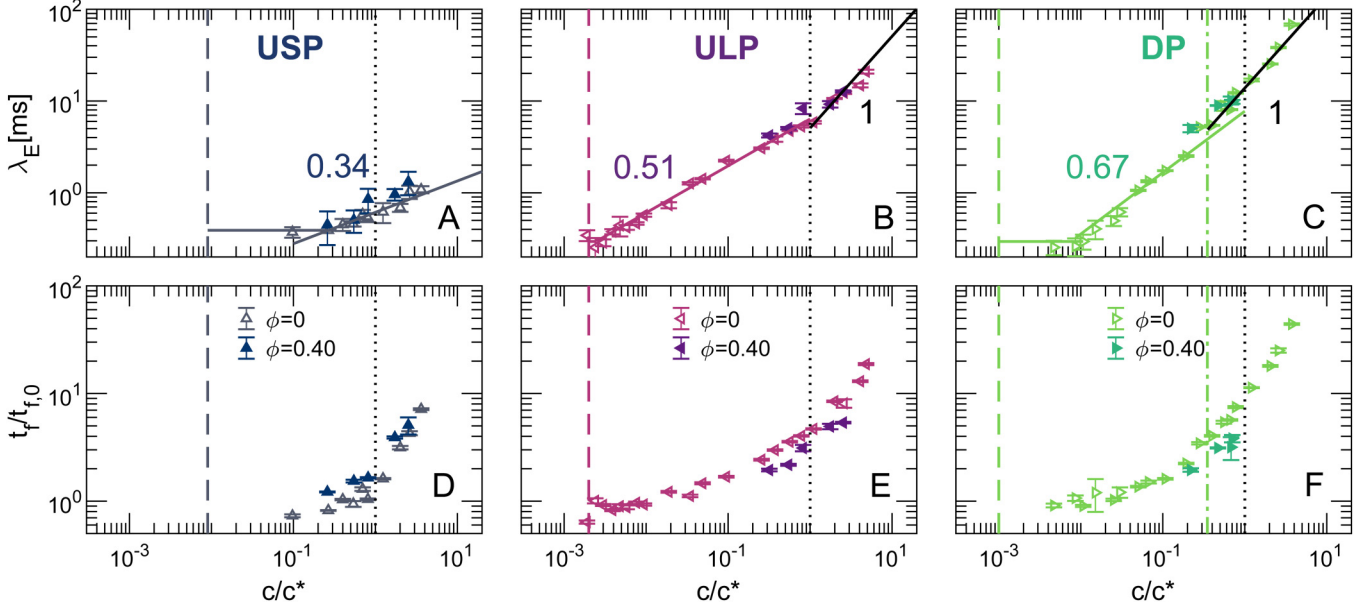


**FIG. 8.** (a)–(c) Extensional relaxation time  $\lambda_E$  for polyacrylamide solutions (open symbols) and  $\phi = 0.40$  depletion suspensions (closed symbols) as a function of normalized polymer concentration  $c/c^*$ . The dashed vertical lines indicate the predicted minimum concentration  $c_{\min}$  needed to observe an elastocapillary response for each polymer. The black dotted vertical lines indicate the transition from the dilute to semidilute regime. For DP solutions, the vertical dashed dotted line indicates the overlap concentration  $c^*$  derived from the Mark–Houwink equation and  $M_w$ . Power-law exponents extracted from the fitting are  $0.34 \pm 0.06$  for USP,  $0.51 \pm 0.02$  for ULP, and  $0.67 \pm 0.07$  for DP. Data for  $\lambda_E$  of polymer solutions without particles are taken from [63]. (d)–(f) Normalized filament lifespan  $t_f/t_{f,0}$  for polyacrylamide solutions (open symbols) and  $\phi = 0.40$  depletion suspensions (closed symbols) as a function of normalized polymer concentration  $c/c^*$ .  $t_f$  for polyacrylamide solutions are normalized with the filament breakup time of 80 (w/w)% glycerol/water,  $t_{f,0} = 10.3$  ms, and  $t_f$  for depletion suspensions are normalized with the filament lifespan of the  $\phi = 0.40$  TtMA suspension,  $t_{f,0} = 29.6$  ms.

the PL and EC scaling regimes, in addition to the regimes of deformation outside of the available models. When  $t_f$  is normalized with the lifespan without polymer addition  $t_{f,0}$  [i.e., the lifespan of the glycerol/water solvent for the polymer solutions and of the  $\phi = 0.40$  suspension without added polymer (NP) for the depletion suspensions],  $t_f/t_{f,0}$  approximately collapses for both polymer solutions and depletion suspensions [Figs. 8(d)–8(f)]. This result indicates that the polymer contributions are similar for both a Newtonian solvent and the dense colloidal suspensions, independent of the dominant physics controlling the filament thinning and pinch-off.

Both  $\lambda_E$  and  $t_f$  are much shorter than the time scales associated with particle diffusion and bond formation (Table IV). Furthermore, the viscous time scale  $t_{vc} = \eta R_0/\sigma$  for the pinching of suspensions ranges between 7 and 40 ms. Thus, comparison of the colloidal and pinching time scales suggests that particle-related dynamics are too slow to affect the pinching process in these mixtures.

#### IV. CONCLUSIONS

We determined the pinch-off dynamics of a dense colloidal suspension and depletion mixtures of colloids and polymers using DoS measurements. In the absence of polymer, a colloidal suspension at volume fraction  $\phi = 0.40$  exhibits multiple linear regimes in the radius evolution scaling. Addition of polymer introduces additional viscoelastic stresses that can influence the radius evolution, often leading to an EC scaling regime in which the radius decays exponentially, allowing the extensional relaxation time to be

computed from the decay constant. An additional regime in which the radius decays linearly with time is due to the interplay of terminal extensional viscosity and capillary effects arising from finite extensibility. The contributions of the polymer to the overall pinch-off depend on the polymer size. The viscous contribution dominates in USP suspensions, whereas the elastic contribution dominates in ULP and DP suspensions. This conclusion is supported by the extensional viscosity  $\eta_E$  profiles, where both extensional thickening  $\eta_{E,\infty}/\eta_{E,0}$  and the Trouton ratio  $\text{Tr}^\infty = \eta_{E,\infty}/\eta_0$  depend on polymer molecular weight: for suspensions containing ULP and DP,  $\text{Tr}^\infty \approx 80$ –140, whereas for USP suspensions,  $\text{Tr}^\infty \approx 8$ –14. Together, these results suggest that there is a molecular weight threshold for polymer additives to fully contribute to the suspension pinch-off dynamics.

The EC regime of suspensions corresponds to that of the polymer solutions. Moreover,  $\lambda_E$  for suspensions and solutions collapses onto universal curves for a given polymer as a function of overlap concentration  $c/c^*$ . Thus, for depletion suspensions, the power-law scaling exponent in the dilute regime is determined by polymer size and the transition concentration from power-law to linear scaling is affected by polymer dispersity, as shown in our previous study for polymer solutions without added particles [63]. This result confirms that the polymer in the interstitial fluid dominates the extensional dynamics. Similarly, the normalized filament lifespan  $t_f/t_{f,0}$  approximately collapses for suspensions and solutions of a given polymer. The dominant role of the polymer in controlling the extensional flow along with the dominant role of the particles in determining the shear response suggests that the shear and extensional responses of



depletion suspensions can be separately tailored through each constituent, as also very recently shown in a microgel/polymer system [97].

Finally, the filament morphology and post-pinch-off behavior of colloid-polymer suspensions differ from those of polymer solutions. Dense suspensions with no polymer and with USP display the conical necks often seen in power-law fluids, whereas ULP and DP exhibit a slender filament typical of elastic fluids. As the filament breaks, however, the colloid-polymer suspensions exhibit recoil, observed in discontinuous shear-thickening fluids, rather than the bead-on-spring structures observed for polymer solutions. In future work, we will explore the effect of polymer size on higher colloidal volume fractions toward the jamming transition.

## ACKNOWLEDGMENTS

The authors thank Megan Robertson for access to the DHR-2 Rheometer, Alamgir Karim for access to the KronTech high-speed camera, Peter Vekilov for access to DLS instrument, Gerald Blosser for machining of the DoS setup, and Christopher Macosko, Randy Ewoldt, Jianyi Du, Jeremy Palmer, and Amanda Marciel for constructive discussions. J.C.C. and D.D.S. acknowledge funding from the National Science Foundation (NSF) (Grant No. CBET-1803728) and the Welch Foundation (No. E-1869). V.S. and C.M. acknowledge funding from PPG Industries for related studies of particle suspensions in viscoelastic fluids and coating formulations.

## AUTHOR DECLARATIONS

### Conflict of Interest

The author have no conflicts to disclose.

## DATA AVAILABILITY

The data that support the findings of this study are available from the corresponding author upon reasonable request.

## NOMENCLATURE

$\mathcal{D}$	dispersity
$k_B T$	energy (Boltzmann constant times temperature)
$M_w$	weight-averaged molecular weight
$R_g$	radius of gyration
$u$	interaction potential

## REFERENCES

- Conrad, J. C., S. R. Ferreira, J. Yoshikawa, R. F. Shepherd, B. Y. Ahn, and J. A. Lewis, "Designing colloidal suspensions for directed materials assembly," *Curr. Opin. Colloid Interface Sci.* **16**, 71–79 (2011).
- Truby, R. L., and J. A. Lewis, "Printing soft matter in three dimensions," *Nature* **540**, 371–378 (2016).
- Roussel, N., "Rheological requirements for printable concretes," *Cem. Concr. Res.* **112**, 76–85 (2018).
- Román-Manso, B., J. Muth, L. J. Gibson, W. Ruettinger, and J. A. Lewis, "Hierarchically porous ceramics via direct writing of binary colloidal gel foams," *ACS Appl. Mater. Interfaces* **13**, 8976–8984 (2021).
- Xu, J., C. Slykas, A. S. Braegelman, K. G. Alvarez, T. Kasl, B. W. Boudouris, M. J. Webber, V. Sharma, and W. A. Phillip, "Heavy metal removal using structured sorbents 3D printed from carbon nanotube-enriched polymer solutions," *Matter* **5**, 3432–3451 (2022).
- Guo, Y., H. S. Patanwala, B. Bognet, and A. W. K. Ma, "Inkjet and inkjet-based 3D printing: Connecting fluid properties and printing performance," *Rapid Prototyping J.* **23**, 562–576 (2017).
- Jimenez, L. N., C. D. V. Martínez Narváez, C. Xu, S. Bacchi, and V. Sharma, "The rheologically-complex fluid beauty of nail lacquer formulations," *Soft Matter* **17**, 5197–5213 (2021).
- Larson, R. G., A. K. Van Dyk, T. Chatterjee, and V. V. Ginzburg, "Associative thickeners for waterborne paints: Structure, characterization, rheology, and modeling," *Prog. Polym. Sci.* **129**, 101546 (2022).
- Crespy, D., K. Friedemann, and A.-M. Popa, "Colloid-electrospinning: Fabrication of multicompartiment nanofibers by the electrospinning of organic or/and inorganic dispersions and emulsions," *Macromol. Rapid Commun.* **33**, 1978–1995 (2012).
- Yu, J., and C.-W. Kan, "Review on fabrication of structurally colored fibers by electrospinning," *Fibers* **6**, 70 (2018).
- Nelson, A. Z., K. S. Schweizer, B. M. Rauzan, R. G. Nuzzo, J. Vermant, and R. H. Ewoldt, "Designing and transforming yield-stress fluids," *Curr. Opin. Solid State Mater. Sci.* **23**, 100758 (2019).
- Ewoldt, R. H., and C. Saengow, "Designing complex fluids," *Annu. Rev. Fluid Mech.* **54**, 413–441 (2022).
- Tanner, R. I., "Rheology of noncolloidal suspensions with non-newtonian matrices," *J. Rheol.* **63**, 705–717 (2019).
- Boelens, A. M. P., J. J. de Pablo, S. Lim, L. Francis, B. Y. Ahn, and J. A. Lewis, "Visualization and simulation of the transfer process of index-matched silica microparticle inks for gravure printing," *AIChE J.* **63**, 1419–1429 (2017).
- Lakhdar, Y., C. Tuck, J. Binner, A. Terry, and R. Goodridge, "Additive manufacturing of advanced ceramic materials," *Prog. Mater. Sci.* **116**, 100736 (2021).
- Valentine, A. D., T. A. Busbee, J. W. Boley, J. R. Raney, A. Chortos, A. Kotikian, J. D. Berrigan, M. F. Durstock, and J. A. Lewis, "Hybrid 3D printing of soft electronics," *Adv. Mater.* **29**, 1703817 (2017).
- Tagliaferri, S., A. Panagiotopoulos, and C. Mattevi, "Direct ink writing of energy materials," *Mater. Adv.* **2**, 540–563 (2021).
- Gholamipour-Shirazi, A., I. T. Norton, and T. Mills, "Designing hydrocolloid based food-ink formulations for extrusion 3D printing," *Food Hydrocoll.* **95**, 161–167 (2019).
- McClements, D. J., "Designing biopolymer microgels to encapsulate, protect and deliver bioactive components: Physicochemical aspects," *Adv. Colloid Interface Sci.* **240**, 31–59 (2017).
- Acosta, M., V. L. Wiesner, C. J. Martinez, R. W. Trice, and J. P. Youngblood, "Effect of polyvinylpyrrolidone additions on the rheology of aqueous, highly loaded alumina suspensions," *J. Am. Ceram. Soc.* **96**, 1372–1382 (2013).
- Rueschhoff, L., W. Costakis, M. Michie, J. Youngblood, and R. Trice, "Additive manufacturing of dense ceramic parts via direct ink writing of aqueous alumina suspensions," *Int. J. Appl. Ceram. Technol.* **13**, 821–830 (2016).
- Corder, R. D., Y.-J. Chen, P. Pibulchinda, J. P. Youngblood, A. M. Ardekani, and K. A. Erk, "Rheology of 3D printable ceramic suspensions: Effects of non-adsorbing polymer on discontinuous shear thickening," *Soft Matter* **19**, 882–891 (2023).
- Pandey, R., and J. C. Conrad, "Effects of attraction strength on micro-channel flow of colloid-polymer depletion mixtures," *Soft Matter* **8**, 10695–10703 (2012).

- [24] McKinley, G. H., “Visco-elasto-capillary thinning and break-up of complex fluids,” *Rheol. Rev.* **3**, 1–48 (2005).
- [25] Clasen, C., P. M. Phillips, L. Palangetic, and J. Vermant, “Dispensing of rheologically complex fluids: The map of misery,” *AIChE J.* **58**, 3242–3255 (2012).
- [26] Dinic, J., C. D. V. Martínez Narváez, and V. Sharma, Rheology of unentangled polymer solutions depends on three macromolecular properties: Flexibility, extensibility, and segmental dissymmetry, in *Macromolecular Engineering* (John Wiley & Sons, Ltd, Chichester, 2022), pp. 1–36.
- [27] Nicolas, M., “Experimental study of gravity-driven dense suspension jets,” *Phys. Fluids* **14**, 3570–3576 (2002).
- [28] Miskin, M. Z., and H. M. Jaeger, “Droplet formation and scaling in dense suspensions,” *Proc. Natl. Acad. Sci. U.S.A.* **109**, 4389–4394 (2012).
- [29] Furbank, R. J., and J. F. Morris, “An experimental study of particle effects on drop formation,” *Phys. Fluids* **16**, 1777–1790 (2004).
- [30] Bertrand, T., C. Bonnoit, E. Clément, and A. Lindner, “Dynamics of drop formation in granular suspensions: The role of volume fraction,” *Granular Matter* **14**, 169–174 (2012).
- [31] Bonnoit, C., T. Bertrand, E. Clément, and A. Lindner, “Accelerated drop detachment in granular suspensions,” *Phys. Fluids* **24**, 043304 (2012).
- [32] van Deen, M. S., T. Bertrand, N. Vu, D. Quéré, E. Clément, and A. Lindner, “Particles accelerate the detachment of viscous liquids,” *Rheol. Acta* **52**, 403–412 (2013).
- [33] Lindner, A., J. E. Fiscina, and C. Wagner, “Single particles accelerate final stages of capillary break-up,” *Europhys. Lett.* **110**, 64002 (2015).
- [34] Thiévenaz, V., S. Rajesh, and A. Sauret, “Droplet detachment and pinch-off of bidisperse particulate suspensions,” *Soft Matter* **17**, 6202–6211 (2021).
- [35] Thiévenaz, V., and A. Sauret, “The onset of heterogeneity in the pinch-off of suspension drops,” *Proc. Natl. Acad. Sci. U.S.A.* **119**, e2120893119 (2022).
- [36] Zhao, H., H.-F. Liu, J.-L. Xu, W.-F. Li, and K.-F. Lin, “Inhomogeneity in breakup of suspensions,” *Phys. Fluids* **27**, 063303 (2015).
- [37] Mathues, W., C. McIlroy, O. G. Harlen, and C. Clasen, “Capillary breakup of suspensions near pinch-off,” *Phys. Fluids* **27**, 093301 (2015).
- [38] Rubio-Rubio, M., W. Mathues, A. Sevilla, and C. Clasen, “One-dimensional modelling of the thinning of particulate suspensions near pinch-off,” *Int. J. Multiphase Flow* **108**, 202–210 (2018).
- [39] Moon, J. Y., S. J. Lee, K. H. Ahn, and S. J. Lee, “Filament thinning of silicone oil/poly (methyl methacrylate) suspensions under extensional flow,” *Rheol. Acta* **54**, 705–714 (2015).
- [40] Moon, J. Y., S. J. Lee, K. H. Ahn, and S. J. Lee, “Heterogeneity in the final stage of filament breakup of silicone oil/pmma suspensions,” *Rheol. Acta* **55**, 91–101 (2016).
- [41] Smith, M. I., R. Besseling, M. E. Cates, and V. Bertola, “Dilatancy in the flow and fracture of stretched colloidal suspensions,” *Nat. Commun.* **1**, 114 (2010).
- [42] Smith, M. I., “Fracture of jammed colloidal suspensions,” *Sci. Rep.* **5**, 14175 (2015).
- [43] Andrade, R. J. E., A. R. Jacob, F. J. Galindo-Rosales, L. Campo-Deaño, Q. Huang, O. Hassager, and G. Petekidis, “Dilatancy in dense suspensions of model hard-sphere-like colloids under shear and extensional flow,” *J. Rheol.* **64**, 1179–1196 (2020).
- [44] Thiévenaz, V., and A. Sauret, “Pinch-off of viscoelastic particulate suspensions,” *Phys. Rev. Fluid* **6**, L062301 (2021).
- [45] Rajesh, S., V. Thiévenaz, and A. Sauret, “Transition to the viscoelastic regime in the thinning of polymer solutions,” *Soft Matter* **18**, 3147–3156 (2022).
- [46] Dai, S., and R. I. Tanner, “Rheology of semi-dilute suspensions with a viscoelastic matrix,” *Rheol. Acta* **59**, 477–486 (2020).
- [47] Dai, S.-C., F. Qi, and R. I. Tanner, “Viscometric functions of concentrated non-colloidal suspensions of spheres in a viscoelastic matrix,” *J. Rheol.* **58**, 183–198 (2014).
- [48] Harich, R., A. Deblais, A. Colin, and H. Kellay, “Depletion forces induce visco-elasto-capillary thinning of non-Brownian suspensions,” *Europhys. Lett.* **114**, 58006 (2016).
- [49] Ock, J. H., J. S. Hong, and K. H. Ahn, “Acceleration of instability during the capillary thinning process due to the addition of particles to a poly (ethylene oxide) solution,” *J. Non-Newton. Fluid Mech.* **258**, 58–68 (2018).
- [50] McIlroy, C., and O. G. Harlen, “Modelling capillary break-up of particulate suspensions,” *Phys. Fluids* **26**, 033101 (2014).
- [51] Bischoff White, E. E., M. Chellamuthu, and J. P. Rothstein, “Extensional rheology of a shear-thickening cornstarch and water suspension,” *Rheol. Acta* **49**, 119–129 (2010).
- [52] Metzner, A. B., “Rheology of suspensions in polymeric liquids,” *J. Rheol.* **29**, 739–775 (1985).
- [53] Shaqfeh, E. S. G., “On the rheology of particle suspensions in viscoelastic fluids,” *AIChE J.* **65**, e16575 (2019).
- [54] Koch, D. L., and G. Subramanian, “The stress in a dilute suspension of spheres suspended in a second-order fluid subject to a linear velocity field,” *J. Non-Newton. Fluid Mech.* **138**, 87–97 (2006).
- [55] Yang, M., and E. S. G. Shaqfeh, “Mechanism of shear thickening in suspensions of rigid spheres in booger fluids. Part I: Dilute suspensions,” *J. Rheol.* **62**, 1363–1377 (2018).
- [56] Yang, M., and E. S. G. Shaqfeh, “Mechanism of shear thickening in suspensions of rigid spheres in booger fluids. Part II: Suspensions at finite concentration,” *J. Rheol.* **62**, 1379–1396 (2018).
- [57] Dai, S., and R. I. Tanner, “Elongational flows of some non-colloidal suspensions,” *Rheol. Acta* **56**, 63–71 (2017).
- [58] Chellamuthu, M., E. M. Arndt, and J. P. Rothstein, “Extensional rheology of shear-thickening nanoparticle suspensions,” *Soft Matter* **5**, 2117–2124 (2009).
- [59] Le Meins, J.-F., P. Moldenaers, and J. Mewis, “Suspensions of mono-disperse spheres in polymer melts: Particle size effects in extensional flow,” *Rheol. Acta* **42**, 184–190 (2003).
- [60] Khandavalli, S., and J. P. Rothstein, “Extensional rheology of shear-thickening fumed silica nanoparticles dispersed in an aqueous polyethylene oxide solution,” *J. Rheol.* **58**, 411–431 (2014).
- [61] Lauser, K. T., A. L. Rueter, and M. A. Calabrese, “Small-volume extensional rheology of concentrated protein and protein-excipient solutions,” *Soft Matter* **17**, 9624–9635 (2021).
- [62] Dinic, J., and V. Sharma, “Flexibility, extensibility, and ratio of kuhn length to packing length govern the pinching dynamics, coil-stretch transition, and rheology of polymer solutions,” *Macromolecules* **53**, 4821–4835 (2020).
- [63] Soetrisno, D. D., C. D. V. Martínez Narváez, V. Sharma, and J. C. Conrad, “Concentration regimes for extensional relaxation times of unentangled polymer solutions,” *Macromolecules* **56**, 4919–4928 (2023).
- [64] Park, N., V. Rathee, D. L. Blair, and J. C. Conrad, “Contact networks enhance shear thickening in attractive colloid-polymer mixtures,” *Phys. Rev. Lett.* **122**, 228003 (2019).
- [65] Park, N., E. J. Umanzor, and J. C. Conrad, “Aqueous colloid+ polymer depletion system for confocal microscopy and rheology,” *Front. Phys.* **6**, 42 (2018).
- [66] Kodger, T. E., R. E. Guerra, and J. Sprakel, “Precise colloids with tunable interactions for confocal microscopy,” *Sci. Rep.* **5**, 14635 (2015).

- [67] Chatterjee, T., A. K. Van Dyk, V. V. Ginzburg, and A. I. Nakatani, "Formulation-controlled positive and negative first normal stress differences in waterborne hydrophobically modified ethylene oxide urethane (heur)-latex suspensions," *ACS Macro Lett.* **6**, 716–720 (2017).
- [68] Lu, P. J., E. Zaccarelli, F. Ciulla, A. B. Schofield, F. Sciortino, and D. A. Weitz, "Gelation of particles with short-range attraction," *Nature* **453**, 499–503 (2008).
- [69] Lekkerkerker, H. N. W., W. C.-K. Poon, P. N. Pusey, A. Stroobants, and P. B. Warren, "Phase behaviour of colloid+ polymer mixtures," *Europhys. Lett.* **20**, 559–564 (1992).
- [70] Ilett, S. M., A. Orrock, W. C. K. Poon, and P. N. Pusey, "Phase behavior of a model colloid-polymer mixture," *Phys. Rev. E* **51**, 1344–1352 (1995).
- [71] Lekkerkerker, H. N., and R. Tuinier, *Colloids and the Depletion Interaction* (Springer, 2011).
- [72] Crocker, J. C., and D. G. Grier, "Methods of digital video microscopy for colloidal studies," *J. Colloid Interface Sci.* **179**, 298–310 (1996).
- [73] Kulicke, W. M., G. Kiss, and R. S. Porter, "Inertial normal-force corrections in rotational rheometry," *Rheol. Acta* **16**, 568–572 (1977).
- [74] Dinic, J., Y. Zhang, L. N. Jimenez, and V. Sharma, "Extensional relaxation times of dilute, aqueous polymer solutions," *ACS Macro Lett.* **4**, 804–808 (2015).
- [75] Dinic, J., L. N. Jimenez, and V. Sharma, "Pinch-off dynamics and dripping-onto-substrate (DoS) rheometry of complex fluids," *Lab Chip* **17**, 460–473 (2017).
- [76] Trujillo-Pino, A., K. Krissian, M. Alemán-Flores, and D. Santana-Cedrés, "Accurate subpixel edge location based on partial area effect," *Image Vis.* **31**, 72–90 (2013).
- [77] Papageorgiou, D. T., "On the breakup of viscous liquid threads," *Phys. Fluids* **7**, 1529–1544 (1995).
- [78] Martínez Narváez, C. D. V., J. Dinic, X. Lu, C. Wang, R. Rock, H. Sun, and V. Sharma, "Rheology and pinching dynamics of associative polysaccharide solutions," *Macromolecules* **54**, 6372–6388 (2021).
- [79] McKinley, G. H., and A. Tripathi, "How to extract the newtonian viscosity from capillary breakup measurements in a filament rheometer," *J. Rheol.* **44**, 653–670 (2000).
- [80] Fardin, M. A., M. Hautefeuille, and V. Sharma, "Spreading, pinching, and coalescence: The ohnesorge units," *Soft Matter* **18**, 3291–3303 (2022).
- [81] Chen, Y.-J., and P. H. Steen, "Dynamics of inviscid capillary breakup: Collapse and pinchoff of a film bridge," *J. Fluid Mech.* **341**, 245–267 (1997).
- [82] Day, R. F., E. J. Hinch, and J. R. Lister, "Self-similar capillary pinch-off of an inviscid fluid," *Phys. Rev. Lett.* **80**, 704–707 (1998).
- [83] Dinic, J., and V. Sharma, "Macromolecular relaxation, strain, and extensibility determine elastocapillary thinning and extensional viscosity of polymer solutions," *Proc. Natl. Acad. Sci. U.S.A.* **116**, 8766–8774 (2019).
- [84] Entov, V. M., and E. J. Hinch, "Effect of a spectrum of relaxation times on the capillary thinning of a filament of elastic liquid," *J. Non-Newton. Fluid Mech.* **72**, 31–53 (1997).
- [85] Pham, K. N., G. Petekidis, D. Vlassopoulos, S. U. Egelhaaf, W. C. K. Poon, and P. N. Pusey, "Yielding behavior of repulsion-and attraction-dominated colloidal glasses," *J. Rheol.* **52**, 649–676 (2008).
- [86] Tokuyama, M., and I. Oppenheim, "On the theory of concentrated hard-sphere suspensions," *Physica A* **216**, 85–119 (1995).
- [87] Cwalina, C. D., and N. J. Wagner, "Material properties of the shear-thickened state in concentrated near hard-sphere colloidal dispersions," *J. Rheol.* **58**, 949–967 (2014).
- [88] Royer, J. R., D. L. Blair, and S. D. Hudson, "Rheological signature of frictional interactions in shear thickening suspensions," *Phys. Rev. Lett.* **116**, 188301 (2016).
- [89] Hsiao, L. C., S. Jamali, E. Glynos, P. F. Green, R. G. Larson, and M. J. Solomon, "Rheological state diagrams for rough colloids in shear flow," *Phys. Rev. Lett.* **119**, 158001 (2017).
- [90] Gopalakrishnan, V., and C. F. Zukoski, "Effect of attractions on shear thickening in dense suspensions," *J. Rheol.* **48**, 1321–1344 (2004).
- [91] Doshi, P., R. Suryo, O. E. Yildirim, G. H. McKinley, and O. A. Basaran, "Scaling in pinch-off of generalized newtonian fluids," *J. Non-Newton. Fluid Mech.* **113**, 1–27 (2003).
- [92] Suryo, R., and O. A. Basaran, "Local dynamics during pinch-off of liquid threads of power law fluids: Scaling analysis and self-similarity," *J. Non-Newton. Fluid Mech.* **138**, 134–160 (2006).
- [93] Huisman, F. M., S. R. Friedman, and P. Taborek, "Pinch-off dynamics in foams, emulsions and suspensions," *Soft Matter* **8**, 6767–6774 (2012).
- [94] Dinic, J., and V. Sharma, "Power laws dominate shear and extensional rheology response and capillarity-driven pinching dynamics of entangled hydroxyethyl cellulose (HEC) solutions," *Macromolecules* **53**, 3424–3437 (2020).
- [95] Dinic, J., M. Biagioli, and V. Sharma, "Pinch-off dynamics and extensional relaxation times of intrinsically semi-dilute polymer solutions characterized by dripping-onto-substrate rheometry," *J. Polym. Sci. Part B: Polym. Phys.* **55**, 1692–1704 (2017).
- [96] Cheal, O., and C. Ness, "Rheology of dense granular suspensions under extensional flow," *J. Rheol.* **62**, 501–512 (2018).
- [97] Sen, S., R. R. Fernandes, and R. H. Ewoldt, "Soft glassy materials with tunable extensibility," [arXiv:2308.14223](https://arxiv.org/abs/2308.14223) [cond-mat.soft] (2023).
- [98] Sur, S., and J. Rothstein, "Drop breakup dynamics of dilute polymer solutions: Effect of molecular weight, concentration, and viscosity," *J. Rheol.* **62**, 1245–1259 (2018).
- [99] See the supplementary material online for protocol and results (Fig. S1) for determining the salt concentration for hard-sphere interactions; description of the free volume calculations; confocal micrographs of depletion suspensions (Fig. S2) and number density fluctuations (Fig. S3); radius evolution fitting in terms of  $1/Oh^2$  (Fig. S4); radius evolution and extensional viscosity for the  $\phi = 0.40$  TtMA suspension radius evolution (Fig. S5); description of the Trouton ratio calculation, including extensional viscosity as a function of Hencky strain (Fig. S6), terminal extensional viscosity (Fig. S7), plateau values of the shear viscosity (Fig. S8), and Trouton ratio as a function of concentration (Fig. S9); Weissenberg number calculations (Fig. S10); and captions for Movies S1–S6.